Journal of Solid State Chemistry **146,** 271–276 (1999)
Article ID jssc.1999.8371, available online at http://www.idealibrary.com on IDEAL®

Structural Characterization of the β-$Cu_2V_2O_7$–α-$Zn_2V_2O_7$ Solid Solution

Michael Schindler[1] and Frank C. Hawthorne

Department of Geological Sciences, University of Manitoba, Winnipeg, Manitoba, Canada R3T 2N2

Received March 18, 1999; accepted May 10, 1999

$(Zn_{2-x}Cu_x)V_2O_7$ solid-solutions were synthesized by heating to 1000°C, cooling to 750°C, and then quenching. Powder-diffraction patterns and the single-crystal structure refinements of $(Cu_{0.56}Zn_{1.44})V_2O_7$, $(Cu_{1.0}Zn_{1.0})V_2O_7$, and $(Cu_{1.53}Zn_{0.47})V_2O_7$ show that the solid-solution series between α-$Zn_2V_2O_7$ and β-$Cu_2V_2O_7$ is complete and that there is no phase transition. With substitution of Zn by Cu^{2+}, *a* and *b* lattice constants increase and decrease, respectively, while *c* lattice constant and cell volume (*V*) do not change. This results from elongation of the (MO_5) square pyramid (M = Zn, Cu^{2+}) and from rotation of the vanadate tetrahedra. In order to form the elongated square-pyramid that must accompany increasing substitution of Zn by Cu^{2+}, the apical *M*–O bond length increases and decreases its incident bond valence at M^{2+}. The resulting bond-valence deficit is compensated by shortening of the equatorial *M*–O bond lengths. The response of the α-$Zn_2V_2O_7$/β-$Cu_2V_2O_7$ framework to the strain produced by elongation of the square pyramid involves coupled clockwise and counter clockwise rotations of the (VO_4) tetrahedra, accounting for the constant cell volumes and increase and decrease of the *a* and *b* lattice constants, respectively. This cooperative response is possible because there are no symmetry restrictions on the rotation of the (VO_4) tetrahedra. © 1999 Academic Press

INTRODUCTION

β-$Cu_2V_2O_7$ was described by Lavaud and Frit (1) as the monoclinic high-temperature phase of α-$Cu_2V_2O_7$ (2). Its structure has space-group symmetry $C2/c$ with $a = 7.685$, $b = 8.007$, $c = 10.09$ Å and $\beta = 110.27°$. The low-temperature modification, α-$Cu_2V_2O_7$, has space-group symmetry $Fdd2$. Frit and Lavaud (1) showed that the reversible phase transition between the α and β phases occurs at 712°C and less readily in the cooling direction $\beta \rightarrow \alpha$, particularly when the compound has been heated to fusion (780°C) before cooling. In both structures, Cu^{2+} is in elongated square-pyramidal coordination (3); the square-pyramids share edges and form chains linked by $[V_2O_7]^{4-}$ groups. The principal structural difference between the two phases involves the arrangements of the $[V_2O_7]^{4-}$ groups which are parallel in $C2/c$ and nonparallel in $Fdd2$. This kind of arrangement results from a reconstructive phase transformation (4). The CuO/V_2O_5 binary phase diagram was investigated by Brisi and Molinari (5) and Fleury (6,7). They found five incongruently melting phases, but neither of them identified β-$Cu_2V_2O_7$. The β-$Cu_2V_2O_7$ phase occurs as the mineral ziesite in the oxidized zone of a fumerole at the Izalco volcano, El Salvador (4).

α-$Zn_2V_2O_7$ is isostructural with β-$Cu_2V_2O_7$ and was first reported by Gopal and Calvo (8). Its structure has space-group symmetry $C2/c$, with $a = 7.429$, $b = 8.340$, $c = 10.098$ Å and $\beta = 111.27°$. The ZnO–V_2O_5 binary system has been investigated intensively (9–12), and it was shown that yellow α-$Zn_2V_2O_7$ is polymorphic with a high-temperature red β-$Zn_2V_2O_7$ modification. The $\alpha \rightarrow \beta$ transition at 615°C is fast and reversible; the high-temperature β-modification is not quenchable (8).

Thortveitite Structure-Type

Both α-$Zn_2V_2O_7$ and β-$Cu_2V_2O_7$ are related to the thortveitite structure-type $M_2T_2O_7$ (M = Sc, Y, Mg, Mn, Co, Ni; T = Si, P). In the structure of thortveitite, $Sc_2Si_2O_7$ (13), space-group symmetry $C2/m$, the M cations are [6]-coordinated and the Si–O–Si angles are 180°. The space group $C2/m$ is a supergroup of $C2/c$ with [$k2$] (k = klassengleich) and $c' = 2c$ (14). The high-temperature β-phases of a number of pyrophosphates with M = Mg, Mn, Cu, and Zn occur in space group $C2/m$, while their low-temperature α-phases have symmetries that are subgroups of $C2/m$. The symmetry reduction is caused by bending of the T–O–T angle ($\approx$ 140–150°) and by different coordination of the M cations ([5] and [6]-coordination). α-$Cu_2P_2O_7$ (15) is isostructural with α-$Zn_2V_2O_7$ and β-$Cu_2V_2O_7$, while α-$Zn_2P_2O_7$ (16) contains M cations in [5]- and [6]-coordination.

[1] To whom correspondence should be addressed.

0022-4596/99 $30.00

Zn–Cu^{2+} Substitution in α-$Zn_2V_2O_7$

Nord and Stefanidis (17) studied the substitution of Zn by Cu, Co, Mg, Ni, Ca, Mn^{2+}, Cd in α-$Zn_2V_2O_7$ at 600°C. They showed that the substitution of Zn^{2+} by Cu^{2+} at 600°C is restricted to 35% and that, with increasing substitution, the *b* lattice constant decreases and the *a* lattice constant increases. Their powder-diffraction patterns of $(Zn_{2-x}Cu_x)V_2O_7$ compounds ($x = 0$–0.7), suggest reduction to triclinic symmetry.

EXPERIMENTAL

Synthesis

$(Zn_{2-x}Cu_x)V_2O_7$ solid-solutions were prepared in evacuated quartz capsules by reaction of the following stoichiometric ratios: $ZnO:CuO:V_2O_5$ = A, 2:0:1; B, 7:1:4; C, 3:1:2; D, 1:1:1; E, 1:3:2; F, 1:7:4; and G, 0:2:1. They reported solidus temperatures of β-$Cu_2V_2O_7$ and α-$Zn_2V_2O_7$ of 780 and 877°C, respectively (5, 9). In order to yield a homogenous melt, all samples were held at 1000°C for three days, slowly cooled to 750°C, and then quenched. All powder samples were characterized with a Phillips PW 1729 diffractometer using Cu*K*α *X*-radiation.

Single-Crystal Studies

Single crystals from the batches C, D, and E were mounted on a Nicolet *R*3*m* automated four-circle diffractometer. Twenty (C), 14 (D), and 28 (E) reflections were centered using graphite-monochromated Mo*K*α *X*-radiation; the resulting cell dimensions are given in Table 1. A total of 376(C), 380(D), and 382(E) symmetry-independent reflections were measured over the range ($3 \le 2\theta \le 60^\circ$) with index ranges $-2 \le h \le 9$, $-2 \le k \le 9$, $-11 \le l \le 11$, according to the method of Burns *et al.* (18). In order to test for violation of the C-centering, no *hkl* index restrictions were imposed in the data collections. The intensity data were corrected for absorption (psi-scan method), Lorentz, polarization, and background effects and reduced to structure factors. A reflection was considered observed if its magnitude exceeded that of five standard deviations above background, based on counting statistics.

Refinement of the Crystal Structures

Scattering curves for neutral atoms, together with anomalous-dispersion corrections, were taken from Cromer and Liberman (19) and Cromer and Mann (20), respectively. The SHELXS system of programs (21) was used for this work.

The structures were refined in space group *C*2/*c* using the positional coordinates of β-$Cu_2V_2O_7$ (1). The final cycles of refinement involved all variable positional parameters, anisotropic-displacement factors, and site-scattering parameters for the *M* sites. The structures converged to *R*-indices of 1.9% (C), 1.1% (D), and 2.0% (E). Final atom positions and anisotropic-displacement factors are listed in Table 2. Selected interatomic distances and angles are shown in Table 3.

Electron-Microprobe Analysis

Subsequent to the collection of the X-ray intensity data, the crystals used for this work were mounted, polished and carbon-coated for chemical analysis with a Cameca SX-50 electron microprobe operating in wavelength-dispersion mode with an excitation voltage of 15 kV and a specimen current of 20 nA. The standards used were $(VO_2)_2P_2O_7$ (V), $CuFeS_2$ (Cu), and gahnite, $ZnAl_2O_4$ (Zn). Data reduction was done according to the $\phi\rho Z$ method (Pouchou and Pichoir (22, 23)), and the chemical composition (mean of three points) is given in Table 1. The unit formulae were calculated on the basis of seven anions.

TABLE 1
Crystal Data, Data-Collection Parameters, and *R* Indices for $(Zn_{2-x}Cu_x)_2V_2O_7$ Compounds

	C: $(Cu_{0.56}Zn_{1.44})V_2O_7$	D: $(Cu_{1.0}Zn_{1.0})V_2O_7$	E: $(Cu_{1.53}Zn_{0.47})V_2O_7$
Crystal size	75 × 60 × 40 μm	63 × 45 × 40 μm	65 × 60 × 40 μm
Space group	*C*2/*c*	*C*2/*c*	*C*2/*c*
Lattice constants	*a* = 7.495(2) Å	*a* = 7.565(2) Å	*a* = 7.639(2) Å,
	b = 8.253(1) Å,	*b* = 8.201(2) Å	*b* = 8.112(3) Å,
	c = 10.113(2) Å	*c* = 10.119(4) Å	*c* = 10.112(3) Å,
	β = 111.35(2)°	β = 110.92(2)°	β = 110.59(2)°
Cell volume	582.62(2) Å^3	586.40(2) Å^3	586.59(2) Å^3
No. of unique $\|F\|$	376	380	382
No. of $\|F_{obs}\| > 5\sigma F$	326	332	329
R (%)	1.9	1.1	2.0
R_w (%)	1.6	1.1	2.05

$R = \sum(|F_o| - |F_c|)/\sum F_o$ $\quad R_w = \sum w(|F_o| - |F_c|)^2/\sum F_o^2)^{1/2}$, $w = 1$

TABLE 2
Atom Positions and anisotropic Atomic Displacement Factors ($\times 10^4$) for C ($(Cu_{0.56}Zn_{1.44})V_2O_7$), D ($(Cu_{1.0}Zn_{1.0})V_2O_7$) and E ($(Cu_{1.53}Zn_{0.47})V_2O_7$)

	x	*y*	*z*	*U*[11]	*U*[22]	*U*[33]	*U*[23]	*U*[13]	*U*[12]
M(C)	0.18296(9)	0.07397(8)	0.98210(6)	21(1)	12(1)	14(1)	− 1(1)	10(1)	− 2(1)
M(D)	0.18520(5)	0.07419(5)	0.98336(3)	27(1)	10(1)	13(1)	− 1(1)	10(1)	− 2(1)
M(E)	0.1872(1)	0.0743(1)	0.98472(7)	26(1)	7(1)	12(1)	− 1(1)	9(1)	2(1)
V(C)	0.2408(1)	− 0.2598(1)	0.79240(8)	10(1)	15(1)	10(1)	2(1)	5(1)	3(1)
V(D)	0.23551(8)	− 0.2655(1)	0.79085(5)	14(1)	13(1)	9(1)	20(2)	52(2)	42(2)
V(E)	0.2297(1)	− 0.2720(1)	0.78905(9)	14(1)	9(1)	8(1)	2(1)	4(1)	3(1)
O1(C)	0	− 0.3187(7)	0.75	12(3)	62(5)	39(3)	0	7(3)	0
O1(D)	0	− 0.3335(4)	0.75	19(2)	59(2)	43(2)	0	13(1)	0
O1(E)	0	− 0.3504(9)	0.75	23(4)	42(5)	38(3)	0	8(3)	0
O2(C)	0.2824(5)	− 0.2352(4)	0.6368(3)	27(2)	26(2)	20(2)	3(2)	9(2)	7(2)
O2(D)	0.2764(3)	− 0.2402(2)	0.6341(2)	32(1)	21(1)	16(1)	3(1)	10(1)	8(1)
O2(E)	0.2708(6)	− 0.2448(6)	0.6313(4)	30(2)	14(2)	20(2)	1(1)	9(2)	6(2)
O3(C)	− 0.1148(5)	0.0925(4)	0.8952(3)	18(2)	24(2)	22(2)	3(2)	5(2)	− 1(2)
O3(D)	− 0.1190(3)	0.09160(2)	0.89520(2)	22(1)	22(1)	18(1)	2(1)	4(1)	1(1)
O3(E)	− 0.1214(5)	0.0895(5)	0.8962(3)	20(2)	22(2)	19(2)	5(2)	6(2)	− 1(2)
O4(C)	0.2766(5)	− 0.0883(4)	0.8815(3)	48(3)	20(2)	31(2)	1(2)	24(2)	9(2)
O4(D)	0.2643(3)	− 0.0913(3)	0.8771(2)	58(1)	21(1)	30(1)	1(1)	28(1)	7(1)
O4(E)	0.2480(6)	− 0.0942(6)	0.8715(4)	48(3)	22(3)	23(2)	0(2)	17(2)	1(2)

RESULTS AND DISCUSSION

Solid-Solution Series

Preparation of the samples A, B, C, D, E, and F gave α-$Zn_2V_2O_7$/β-$Cu_2V_2O_7$ solid solutions with small impurities of synthetic fingerite $Cu_{11}O_2(VO_4)_6$ (24). Sample **G** gave either α-$Cu_2V_2O_7$ or mixtures of α-$Cu_2V_2O_7$ and β-$Cu_2V_2O_7$. The latter result shows that the presence of Zn seems to inhibit formation of α-$Cu_2V_2O_7$.

The powder-diffraction patterns of B, C, D, E, and F contain no reflections that violate space-group symmetry $C2/c$ or indicate a supercell of α-$Zn_2V_2O_7$. The correct space-group symmetry and cell are confirmed by the low *R*-indices in the single-crystal structure refinements. Our results show

TABLE 3
Selected Bond Distances (Å) and Angles (°) in $(Zn_{2-x}Cu_x)_2V_2O_7$ Phases

	α-$Zn_2V_2O_7$	$(Cu_{0.56}Zn_{1.44})V_2O_7$	$(Cu_{1.0}Zn_{1.0})V_2O_7$	$(Cu_{1.53}Zn_{0.47})V_2O_7$	β-$Cu_2V_2O_7$
M–O4	1.988(6)	1.981(3)	1.953(2)	1.941(4)	1.930(5)
M–O2a	1.988(6)	1.960(3)	1.976(2)	1.963(4)	1.944(5)
M–O3a	2.088(6)	2.037(3)	2.012(2)	1.974(4)	1.937(5)
M–O2b	2.087(6)	2.055(3)	2.015(2)	1.973(4)	1.950(5)
M–O3b	2.027(6)	2.085(3)	2.155(2)	2.211(3)	2.259(5)
⟨*M*–O⟩	2.036(6)	2.024(3)	2.022(2)	2.012(4)	2.004(5)
V–O4	1.658(8)	1.647(3)	1.648(2)	1.647(5)	1.644(6)
V–O3	1.704(7)	1.708(3)	1.694(2)	1.692(4)	1.694(4)
V–O2	1.728(4)	1.724(3)	1.734(2)	1.745(4)	1.741(4)
V–O1	1.775(4)	1.765(2)	1.769(1)	1.775(3)	1.770(4)
⟨V–O⟩	1.716(6)	1.711(3)	1.711(2)	1.715(4)	1.712(4)
V–O1–V	149(1)	148.0(4)	143.3(2)	138.0(4)	132.0(5)
V–O2a–*M*	131.3(3)	131.2(2)	131.4(1)	131.6(2)	131.5(3)
V–O2b–*M*	122.2(4)	123.2(2)	124.0(1)	124.6(2)	124.9(3)
V–O3a–*M*	128.2(2)	127.5(2)	126.9(1)	125.4(2)	121.1(2)
V–O3b–*M*	130.8(3)	130.7(2)	131.6(1)	132.6(2)	136.2(2)
V–O4–*M*	144.7(2)	148.6(2)	152.3(1)	156.9(2)	157.8(3)

that the solid-solution series between α-$Zn_2V_2O_7$ and β-$Cu_2V_2O_7$ is complete and there is no phase transition under the conditions examined.

Distortion of the Framework

Figure 1 shows the change in the *a* and *b* lattice constants with variation in chemical composition. The structural data for the end-members α-$Zn_2V_2O_7$ and β-$Cu_2V_2O_7$ were taken from Lavaud and Frit (1) and Gopal and Calvo (8). The variation in *a* and *b* is uniform and confirms a complete solid solution with no phase transition. The variations of the *c* lattice constant (10.098–10.119 Å) and the cell volume (582.6–586.4 Å^3) are minimal. The near-constant value of *V* with large changes in *a* and *b* result from elongation of the (MO_5) square pyramid (M = Zn, Cu^{2+}) and from rotation of the vanadate tetrahedra (Figs. 2 and 3, Table 3).

(MO_5) Coordination Polyhedron

The mineral ziesite has the structure of β-$Cu_2V_2O_7$ and is one of sixteen Cu^{2+}-oxysalt minerals containing Cu^{2+} in [5]-coordination (3). Eby and Hawthorne (25) have shown that Cu^{2+} in minerals occurs more often in square-pyramidal than triangular-bipyramidal coordination. They did not find a continuous transitional path between the two coordinations in minerals, whereas Effenberger (26) showed a continuous transition between the two coordinations for a wider range of inorganic compounds. Hartree-Fock calculations for (CuO_5) polyhedra (3) indicate that the compressed triangular-bipyramid is of lower energy than the elongated triangular-bipyramid, and the elongated square-pyramid has lower energy than the compressed square-pyramid. The Hartree-Fock calculations also indicate that the compressed triangular-bipyramid is more energetically favorable than the elongated square-pyramid, despite the fact that square-pyramidal coordination occurs more often in minerals. The ground states of Cu^{2+} in triangular-bipyramidal and square-pyramidal coordination do not contain energetically degenerate electronic states, and there is no Jahn–Teller effect. However, Reinen and Atansov (27) have argued that vibronic interaction between the ground state and the excited state leads to stabilization of the elongated square-pyramid, as the excited state is

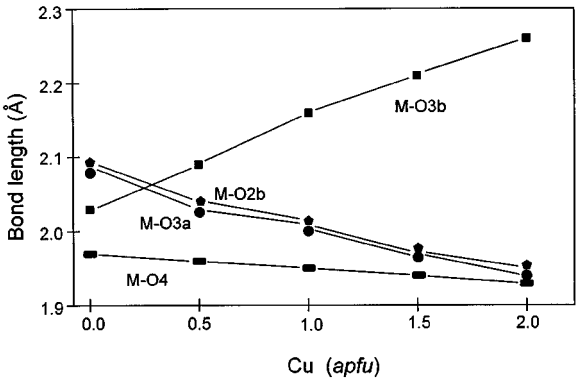

FIG. 2. Lengthening of the apical *M*–O3b bond and shortening of the equatorial *M*–O3a, *M*–O2b, and *M*–O4 bonds with increasing substitution of Zn by Cu^{2+} (in apfu of Cu^{2+}).

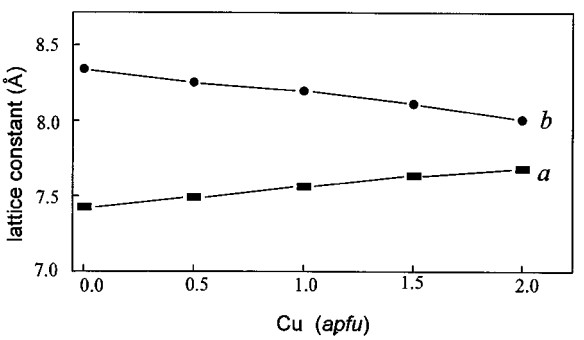

FIG. 1. Variation in *a* and *b* lattice constants with increasing substitution of Zn by Cu^{2+} (in apfu of Cu^{2+}) in square-pyramidal coordination in the $(Zn_{2-x}Cu_x)_2V_2O_7$ phases.

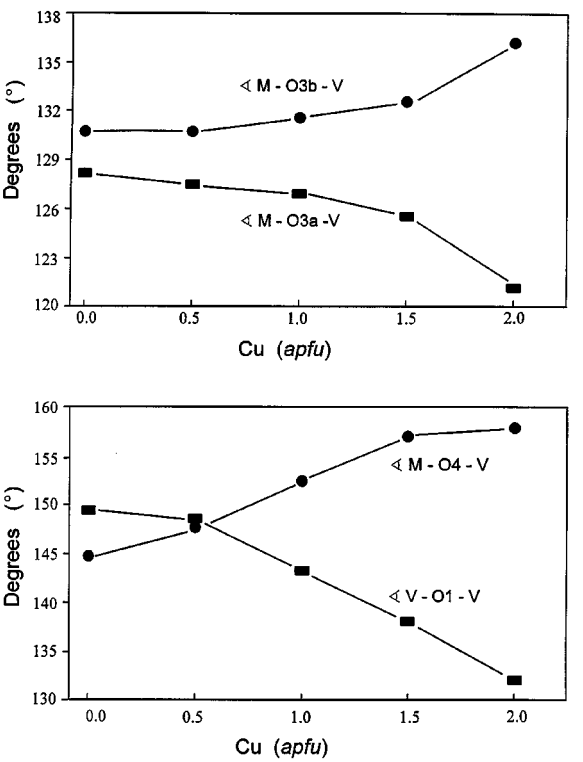

FIG. 3. Variation in the *M*–O–V and V–O–V angles with increasing substitution of Zn by Cu^{2+} (in apfu of Cu^{2+}).

Jahn–Teller active. Therefore, a *quasi-Jahn–Teller effect* in Cu^{2+} square-pyramidal coordination may lead to a net stabilization of elongated square-pyramidal coordination.

Zn^{2+} has no energetically degenerate electronic ground states and (ZnO_n) polyhedra have no internal driving mechanism for distortion of the holosymmetric arrangments. In α-$Zn_2V_2O_7$, the square pyramid around Zn is slightly distorted with a range in bond lengths from 1.973 to 2.088 Å (Table 3). In order to form the energetically favored elongated square-pyramid that must accompany increasing substitution of Zn by Cu^{2+}, the apical *M*1a–O3b bond length increases from 2.027(4) in α-$Zn_2V_2O_7$ to 2.258(3) Å in β-$Cu_2V_2O_7$ (Figs. 2 and 3). Accordingly, the equatorial bond lengths *M*1a–O3a, *M*1a–O4, *M*1a–O2a, and *M*1a–O2b shrink from 1.973–2.088 Å in α-$Zn_2V_2O_7$ to 1.930–1.948 Å in β-$Cu_2V_2O_7$ (Table 3, Fig. 2). Lengthening of the apical *M*1a–O3b bond produces an incident bond-valence deficit at M^{2+}; this deficit is compensated by shortening of the equatorial *M*–O bond lengths. This process of elongation and compression is continuous across the solid-solution series (Fig. 2, Table 3) and is confirmed by small anisotropic atomic-displacement factors for O3 (Table 2).

Rotation of the (V_2O_7) Group

The elongation of the (Zn, $Cu^{2+}O_5$) square pyramid is parallel to *a* and the contraction of the four equatorial bond lengths is parallel to *b* (Fig. 4). In the three-dimensional framework, lengthening of the *M*1a–O3b bond causes clockwise rotation of the central ($V1aO_4$) tetrahedron in the *ab*-plane. This rotation occurs around the *M*–O2–V axis which is perpendicular to the *ab*-plane; it increases the angles *M*1a–O3b–V and *M*1a–O4–V and decreases the angles *M*1b–O3b–V and V1a–O1–V1b while the *M*–O2–V angle remains constant (Figs. 3 and 4, Table 3). The decreasing V1a–O1–V1b angle causes a counterclockwise rotation of the ($V1bO_4$) tetrahedron around the same axis (Fig. 4). Thus, the response of the α-$Zn_2V_2O_7$/β-$Cu_2V_2O_7$ framework to the strain produced by elongation of the square pyramid involves coupled clockwise and counterclockwise rotation of the (VO_4) tetrahedra, accounting for the near-constant cell volumes and the increase and decrease in *a* and *b* respectively. This elastic response is possible because there are no symmetry restrictions on rotation of the (VO_4) tetrahedra.

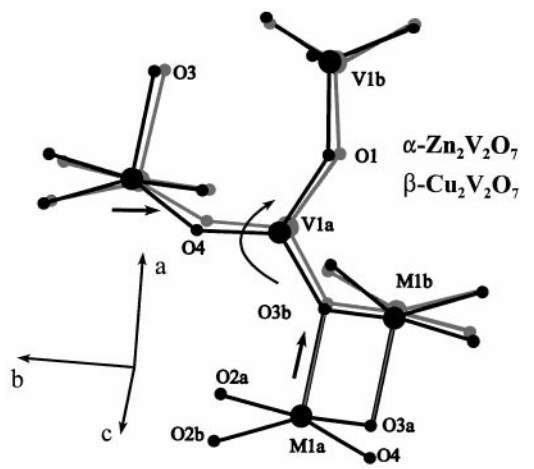

FIG. 4. The environment of the V1a tetrahedron in the direction of the *M*–O2–V axis in α-$Zn_2V_2O_7$ and β-$Cu_2V_2O_7$. It is apparent that, with lengthening of the *M*–O3b bond, the ($V1aO_4$) tetrahedron begins to rotate clockwise in the *ab*-plane. This rotation decreases the V1a–O1–V1b angle which causes counterclockwise rotation of the ($V1bO_4$) tetrahedron. Atoms and bonds in α-$Zn_2V_2O_7$ are black and in β-$Cu_2V_2O_7$ are gray. O atoms are drawn as small circles and V, Zn, and Cu atoms are drawn as large circles.

Comparison with the Adamite–Olivenite Solid-Solution Series

In adamite, $Zn_2AsO_4(OH)$, and olivenite, $Cu_2^{2+}AsO_4(OH)$, Cu^{2+} and Zn are both in [5]- and [6]-coordination. Adamite has space-group symmetry *Pnnm* (28) and olivenite has space-group symmetry $P2_1/n$ (29,30). In both structures, the octahedral coordination is a distorted [4 + 2]-coordination with four short equatorial bonds and two long apical bonds. In adamite, Zn is in slightly distorted triangular-bipyramidal coordination, whereas in olivenite, Cu^{2+} is in compressed triangular-bipyramidal coordination. In these structures, initial substitution of Zn by Cu^{2+} occurs in the distorted octahedral coordination and causes slight lengthening of the apical *M*–O bond (M = Zn, Cu^{2+}) (31). Further substitution of Zn by Cu^{2+} incorporates Cu^{2+} into the triangular bipyramid. This leads to formation of the energetically favored compressed triangular-bipyramidal coordination. The phase transition occurs at $\sim$1.6 Cu^{2+} apfu (atoms per formula unit). In adamite, space group *Pnnm*, the O3 atom is both an equatorial and an apical O-atom of the triangular bipyramid. Increasing substitution of Zn by Cu^{2+} in the triangular bipyramid causes lengthening and shortening of the corresponding *M*–O3 bonds, respectively, but in contrast to the α-$Zn_2V_2O_7$/β-$Cu_2V_2O_7$ solid-solution series, the symmetry reduces and the O3 site splits into two symmetrically distinct sites. The reason for this symmetry reduction involves the constraints exerted by the higher space-group symmetry *Pnnm*, as in this space group, three out of four O atoms are on special positions and this strongly constrains possible rotations of the polyhedra.

ACKNOWLEDGMENTS

We thank Peter C. Burns and Mark Cooper for discussions. This work was supported by the Natural Sciences and Engineering Research Council of Canada grants to FCH.

REFERENCES

1. D. Mercurio-Lavaud and M. B. Frit, *C. R. Acad. Sci. Paris*, *C* **277,** 1101 (1973).
2. C. Calvo and R. Faggiani, *Acta Crystallogr. B* **31,** 603 (1975).
3. P. C. Burns, Ph.D. Thesis, University of Manitoba, 1994.
4. J. M. Hughes and R. W. Birnie, *Am. Miner.* **65,** 1146 (1980).
5. C. Brisi and A. Molinari, *Ann. Chim.* **48,** 263 (1958).
6. P. Fleury, C. R. Acad. *Sci. Paris*, *Ser. C*., **263,** 1375 (1966).
7. P. Fleury, Rev. *Chim. Mineral.* **6,** 819 (1969).
8. R. Gopal and C. Calvo, *Can. J. Chem.* **51,** 1004 (1973).
9. A. J. Pollard, U. S. Dept. Commer. Off. Tech. Serv. **AD 412635** (1963).
10. J. J. Brown and F. A. Hummel, *Trans. Brit. Ceram. Soc.* **64,** 419 (1965).
11. J. Argenault, Rev. *Chem. Miner.* **7,** 651 (1970).
12. V. A. Makarov, A. A. Fotiev, and N. Serebryakova. *Russ. J. Inorg. Chem.* **16,** 1515 (1971).
13. R. Bianchi, T. Pilati, V. Diella, C. M. Gramaccioli, and G. Mannucci, *J. Solid State Chem.* **73,** 601 (1988).
14. "International Tables for Crystallography," Vol. A, Reidel, Dordrecht, 1983.
15. H. Effenberger, *Acta Crystallogr. C* **46,** 691 (1990).
16. B. E. Robertson and C. Calvo, *J. Solid State Chem.* **1,** 120 (1970).
17. A. G. Nord and T. Stefanidis, *Mater. Res. Bull.* **20,** 845 (1985).
18. P. C. Burns, D. J. Mac Donald, and F. C. Hawthorne, *Can. Mineral.* **32,** 31 (1994).
19. D. T. Cromer and D. Liberman, *J. Chem. Phys.* **53,** 1891 (1970).
20. D. T. Cromer and J. B. Mann, *Acta Crystallgr. A* **24,** 321 (1968).
21. G. M. Sheldrick, A Crystallographic Computing Package (revision 4.1), Siemens Analytical X-Ray Instruments., Madison, Wisconsin (1990).
22. J. L. Pochou and F. Pichoir, *La Recherche Aerosp.* **3,** 13 (1984).
23. J. L. Pochou and F. Pichoir, *Microbeam Anal.*, 104, (1985).
24. J. M. Hughes and C. G. Hadidiacos, *Am. Miner.* **70,** 193 (1985).
25. R. K. Eby and F. C. Hawthorne, *Acta Crystallogr. C* **46,** 2291 (1990).
26. H. Effenberger, *J. Solid State Chem.* **73,** 118 (1988).
27. D. Reinen and M. Atanasov, *Chem. Phys.* **136,** 27 (1989).
28. F. C. Hawthorne, *Can. Mineral.* **14,** 143 (1976).
29. K. Toman, *Acta Crystallogr. B* **33,** 2628 (1977).
30. P. C. Burns and F. C. Hawthorne, *Can. Mineral.* **33,** 885 (1995).
31. K. Toman, *Acta Crystallogr. B* **34,** 714 (1978).